Hindawi
Mathematical Problems in Engineering
Volume 2023, Article ID 2482533, 14 pages
https://doi.org/10.1155/2023/2482533

*Research Article*

# Performance Improvement of Hybrid System Using Bidirectional MIEC for Portable Device Charger

**S. Rathinamala,[1] S. Manoharan,[2] S. Chandrakala,[1] and K. Ramash Kumar[3]**

[1]*Department of Electrical and Electronics Engineering, KIT-Kalaignarkarunanidhi Institute of Technology, Coimbatore, India*
[2]*Department of Electrical and Electronics Engineering, JCT College of Engineering and Technology, Coimbatore, India*
[3]*Department of Electrical and Electronics Engineering, Dr. N.G.P. Institute of Technology, Coimbatore-48, Tamilnadu, India*

Correspondence should be addressed to K. Ramash Kumar; ramashkumar@drngpit.ac.in

Received 19 May 2023; Revised 25 July 2023; Accepted 8 September 2023; Published 30 September 2023

Academic Editor: Alessandro Lo Schiavo



In this paper, a novel bidirectional multi-input energy harvesting converter (MIEC) for portable device charger is presented. Switches that are separately regulated using different duty ratios are used in the design of such an MIEC power converter. The peak power of the photovoltaic sources may be tracked using such duty ratios, and the battery power can also be managed. The switch with two directions is also a part of this converter. If necessary, the battery can be charged via a USB charger but it is also capable of supplying power to the portable charging devices using sun and vibration harvesting. A battery receives the remaining energy for recharging while the charging current level can be checked. The entire system built using the MATLAB/SIMULINK environment, performances are monitored by the simulation results and validated experimentally.

## 1. Introduction

Now days uses of modern technological products particularly portable devices consume more power, because of frequent charging [1]. Therefore, alternative energy sources are needed to provide a reliable power supply [2]. Now a days photovoltaic (PV) chargers for mobile phones are available in the market, which are suitable only for recharge during a day. Therefore the combination of two or more energy sources is the solution for getting continuous power supply. The photovoltaic cell and vibration generator were considered to harvest require power source with a magnitude of at least several milliwatts to recharge the portable devices properly [3, 4]. It requires designing and fabricating a multiple input hybrid energy harvesting system that integrates both vibration generators and solar panels, enabling energy harvesting from vibration and light simultaneously which includes energy storage elements (battery).

In the earlier investigations, the DC-–DC converter is used as a multiple-input energy harvesting circuit. A dual input converter topology presented by Shukman [5] and Thakur and Patel [6] can be operated in buck, buck–boost, and boost modes of operation and it offers compact design with series and parallel combination of connected sources, but there is no bidirectional port to interface the battery. A multiple-input converter based on a boost topology is presented by Solero et al. [7], Rathinamala and Manoharan [8], Aymen [9], and Cheng et al. [10] is suitable for the large current applications such as hybrid vehicles, because it has lower input current ripple. The basic hybrid systems with individual input harvesting methods reported by Femia et al. [11], Chen and Rincon-Mora [12], Chao et al. [13], and Kim et al. [14] are complex in the system topology, more number of power devices, more power loss, and more setup cost and huge in size. The key drawbacks of processing individual inputs using multiple energy conversion stages are replaced by the hybrid energy harvesting approach in single stage. Hence, the proposed single-stage bidirectional hybrid energy harvesting system to be developed which includes the ability of bidirectional power flow [15–20] which combine different power sources in a single power structure. Therefore, the portable charge device [21–25] directly through a hybrid energy harvesting system, unless otherwise the internal battery present in the converter design to be charged through the USB charger during the unavailability of energy sources. The

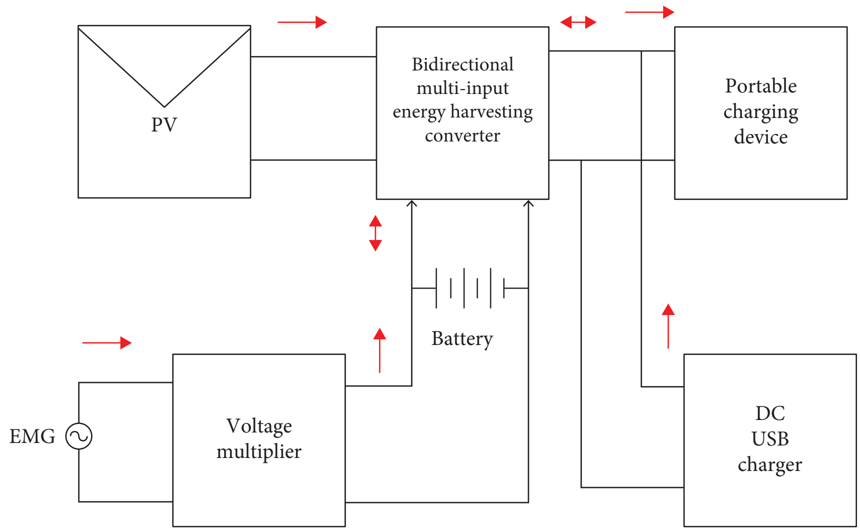


Figure 1: Block diagram of the hybrid system using bidirectional MIEC.

charging system presents in the proposed system allows the battery to charge in the constant current (CC) as well as constant voltage (CV) mode [26–32].

The main contribution of this proposed research work is to design and analyze the performance of a portable device battery charger which ensures protection of battery and complies with all the charging procedures. Also this paper compares the hardware design and simulation performance of the portable battery charger system. Section 1 deals about the introduction and literatures of the converter. Section 2 explains the working of the proposed MIES converter circuit. Section 3 discusses about the control methodology of the proposed model. Section 4 discusses simulation and experimental findings and Section 5 illustrates the conclusion of the proposed system.

## 2. System Architecture

The purpose of the bidirectional multi-input energy harvesting converter (MIEC) presented in the paper is to serve as a novel portable device charger. It utilizes separately regulated switches with different duty ratios to efficiently manage power from photovoltaic sources and a battery. The converter is designed to track the peak power of the photovoltaic sources, manage battery power, and enable charging of the battery via a USB charger. Additionally, an MIEC can harness solar and vibration energy for powering portable charging devices (PCDs). The system's performance is evaluated by the simulations conducted in the MATLAB/SIMULINK environment and validated experimentally. The block diagram of the bidirectional multi-input hybrid energy harvesting system for portable device charger is shown in Figure 1. This system consists of bidirectional MIEC and voltage multiplier.

The power converter is designed to deliver the required power to the portable device charger through the solar and vibration harvester directly or through the internal battery. Whether the energy sources are unavailable or lessen the value, the converter able to charge the internal battery through the USB DC supply.

The internal circuit diagram of the proposed converter for USB is shown in Figure 2, which includes the MIEC and active diode-based voltage multiplier to harvest the energy from vibration. Figure 3 illustrates the proposed bidirectional MIEC along with the circuit diagram of the DC USB charger. A dual-input converter as well as the battery source that comprises of three active switches $S_1$, $S_2$, and $S_3$; two inductors $L_1$ and $L_2$; and the diode $D_1$. Switches $S_1$ and $S_2$ are controlled through a single control signal. The switch $S_3$ controlled by DC USB. The proposed bidirectional MIEC offers a control regulated and highly efficient output.

The switching cycle waveforms for the entire period are shown in Figure 4. The gate pulses of the switches $S_1$ and $S_3$ are also shown in Figure 4. Initially, the switch $S_1$ is in ON state, the inductor current $i_{L_1}$ charges linearly from period 0 to $t_1$. After $t_1$, the switch $S_1$ is in OFF state, and the inductor current $i_{L_1}$ is discharged up to $t_2$. During $t_2$–$t_3$, the remaining inductor current $i_{L_1}$ is discharged gradually.

Simultaneously at $t_0$, the switch $S_3$ is ON state, the inductor current $i_{L2}$ obtains the charges from the period $t_0$–$t_2$. There is an increase in the charging state shown in Figure 4. After $t_2$ both the switches $S_1$ and $S_3$ goes to OFF condition, hence discharging of inductor currents $i_{L1}$ and $i_{L2}$ occurs in this period. During $t_1$–$t_3$, the switch $S_3$ in the OFF state, therefore the diode $D_1$ is forward biased, it leads to discharge the inductor current to the battery. Figure 5(a)–5(d) illustrates the mode diagrams of all the four nodes of operation of bidirectional energy harvesting converter. The bidirectional MIEC described in this paper employs switches with different duty ratios to regulate the power from various sources. It allows for efficient tracking of the peak power of he photovoltaic sources, such as solar panels, while also managing the power from the battery. The MIEC can charge the battery using a USB charger when necessary and it can also harness

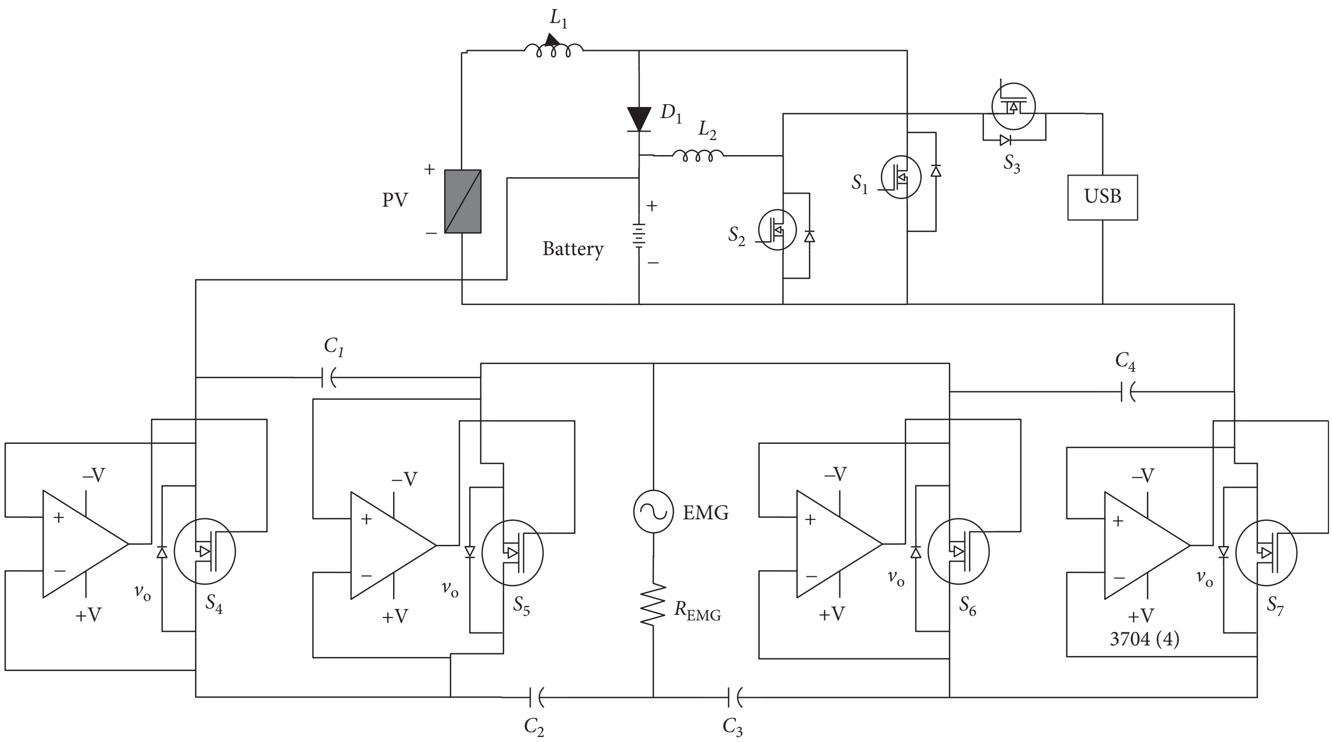


FIGURE 2: Internal circuit structure of proposed model.

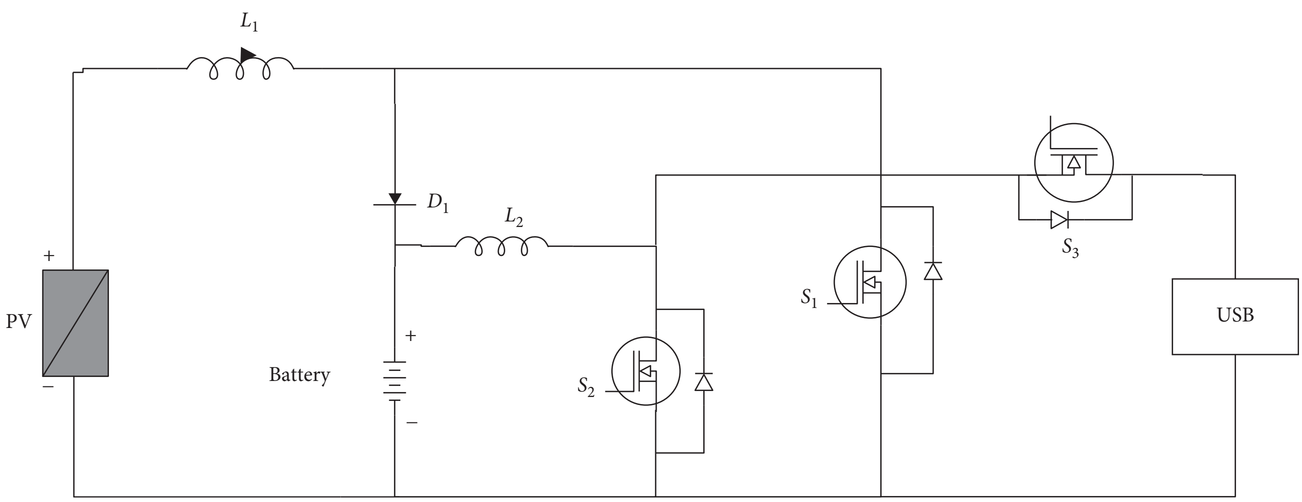


FIGURE 3: The proposed bidirectional multiple input energy harvesting converter.

solar and vibration energy to power PCDs. The converter ensures that the battery receives the remaining energy for recharging, and the charging current level can be monitored as well.

*2.1. Modes of Operation in Bidirectional MIEC.* There are four different modes of operation in MIEC. They are Mode 0, Mode 1, Mode 2, and Mode 3.

Mode 0

In this mode the switches $S_1$ is ON and $S_3$ is OFF. The PV panel's current charges the inductor $L_1$, and flows through the drain–source of the switch $S_{1.}$ and neutralized at PV. At this point, PV power stored in the inductor $L_1$, and the charging current $i_{L_1}$ increases linearly. At the same time, the battery charged through the energy stored in the inductor $L_2$. The inductor current $i_{L_2}$ flows through the battery and body diode of switch $S_2$, as shown in Figure 5(a). The switch $S_1$ is ON according to the maximum power point tracking (MPPT), and the complete PV power is drawn by the inductor $L_1$.

The energy stored in the inductor $L_1$ and $L_2$ can be expressed in Equations (1) and (2)

$$V_{L1} = V_{PV}, \tag{1}$$

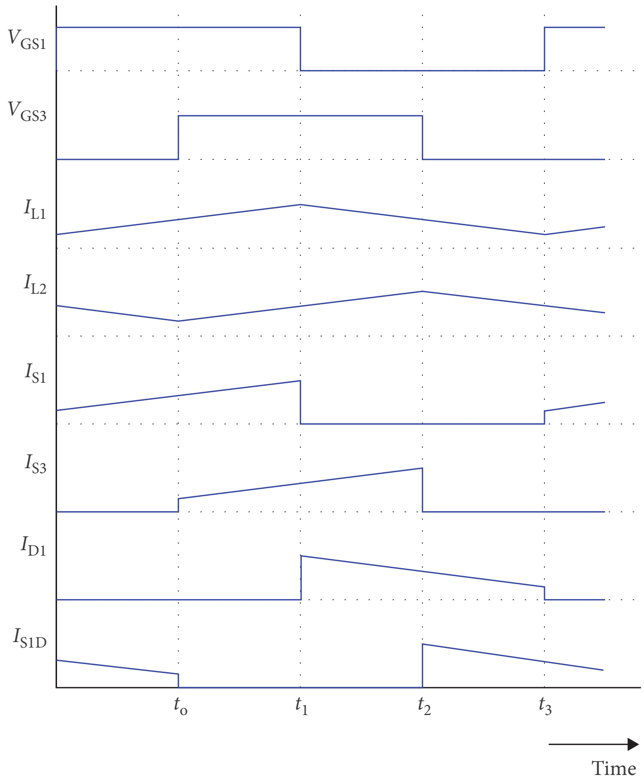


Figure 4: Switching cycle of bidirectional multiple input energy harvesting converter.

$$V_{L2} = -V_{bat}. \quad (2)$$

Mode 1

The switch $S_3$ has been changed to ON mode, and the switch $S_1$ remains ON. The PV panel loads the inductor $L_1$ which passes into the $S_1$ drain–source and is neutralized into the PV. The PV power saved in the inductor, i.e., $L_1$ is now increases linearly with the charging current $i_{L_1}$. At the same time, as seen in Figure 5(b), the USB power charge the inductor by $L_2$ and the battery by switch $S_3$. The ON/OFF control of $S_1$ is based on the PV power. When the charger connected to the USB $S_3$ has switched ON.

The energy stored in the inductors $L_1$ and $L_2$ can be expressed in Equations (3) and (4).

$$V_{L1} = V_{PV}, \quad (3)$$

$$V_{L2} = V_{USB} - V_{bat}. \quad (4)$$

Mode 2

In this mode, switch $S_3$ remains ON and $S_1$ and $S_2$ goes to the OFF state. The USB power charges the inductor $L_2$ and the battery through the switch $S_3$, as shown in Figure 5(c). Simultaneously the power received from PV and the energy stored in the inductor $L_1$ discharged to the battery through diode $D_1$. Equations (5) and (6) represent the expression for voltage across the inductors $L_1$ and $L_2$, respectively.

$$V_{L1} = V_{PV} - V_{bat}, \quad (5)$$

$$V_{L2} = V_{USB} - V_{bat}. \quad (6)$$

Mode 3

All three switches are in OFF state and diode $D_1$ in forward biased. Therefore, energy contained in the inductor $L_1$ and PV power discharges to the battery. At the same time, inductor $L_2$ charges the battery via the body's diode of switch $S_2$ and the flow of inductive current $i_{L2}$ is shown in Figure 5(d). Equations (7) and (8) represent the expression for voltage across the inductors $L_1$ and $L_2$, respectively.

$$V_{L1} = V_{PV} - V_{bat}, \quad (7)$$

$$V_{L2} = -V_{bat}. \quad (8)$$

*2.2. Operation of Active Diode-Based Voltage Multiplier.* The energy harvested from the electromagnetic generator (EMG) has sinusoidal in nature applied to the active diode-based voltage multiplier. The power requirement for active diodes in the voltage multiplier expected to be small; the external power source must still be considered. Here the battery supplies voltage to the comparator present in the voltage multiplier to enables AC/DC conversion. The DC output voltage of the EMG has four times of the input amplitude. The battery will be charged, when the charging current is greater than that of the comparators' supply current. For practice, the battery discharge limit could be set, such that the active diode is activated with an appropriate voltage.

## 3. Control Strategy of Bidirectional MIEC for Portable Device Charger

The control strategy for the proposed converter is shown in Figure 6. An overall control system used to provide MPPT for MIEC regulates the output voltage. In this work, the perturb and observe (P&O) algorithm found the best choice to implement the MPPT. In this strategy, the switch $S_1$ is controlled by the duty ratio $d_1$, which is to be yield the MPPT. The switch $S_3$ controlled by the duty ratio $d_3$ for charging the battery from DC USB power and the duty ratio $d_2$ controlled the switch $S_2$ for charging and discharging the battery.

A two-stage charge management technique is employed for controlling the portable device charging. If a battery for a mobile device is found to be in an undercharged state, causing it to charge 90% of the battery charge level. In CC mode of charging the battery, the proportional–integral (PI) controller limit the average charging level for the battery. After that the battery keeps on charging with CV mode. If the battery reaches its charge level, the controller disconnects the battery from overcharging. The CC–CV charging limit for the lithium-ion battery is shown in Figure 6. In this control structure, the controller enables the current signal received from the battery, and it provides the duty ratio $d_3$

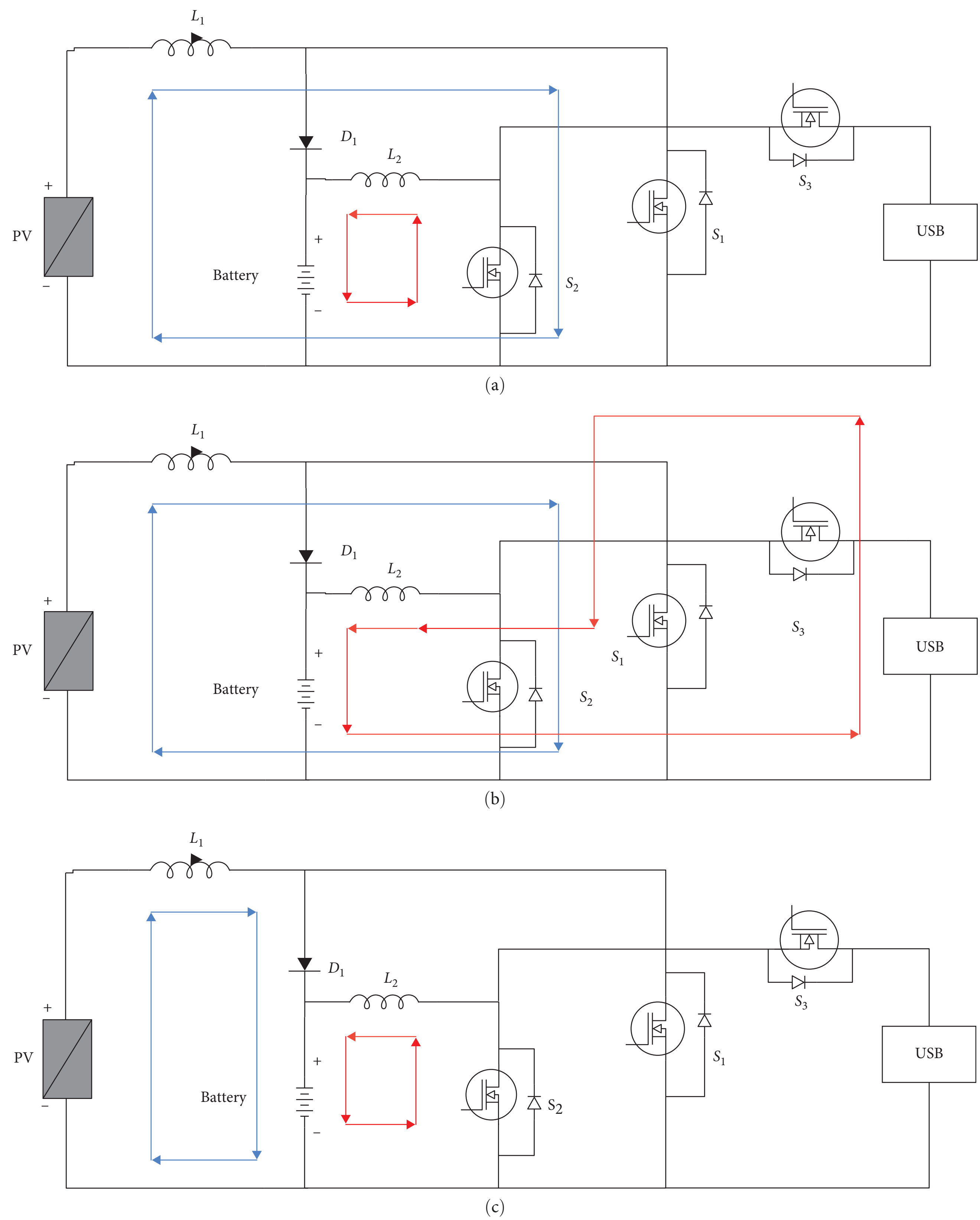


Figure 5: Continued.

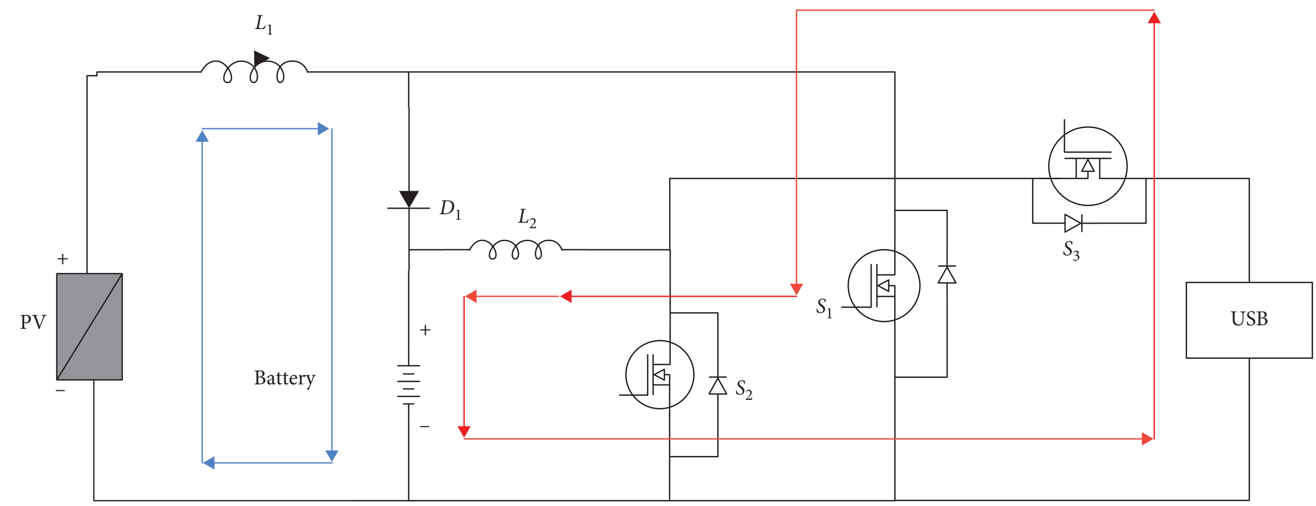


(d)

Figure 5: Mode diagram of bidirectional multiple input energy harvesting converter: (a) Mode 0, (b) Mode 1, (c) Mode 2, and (d) Mode 3.

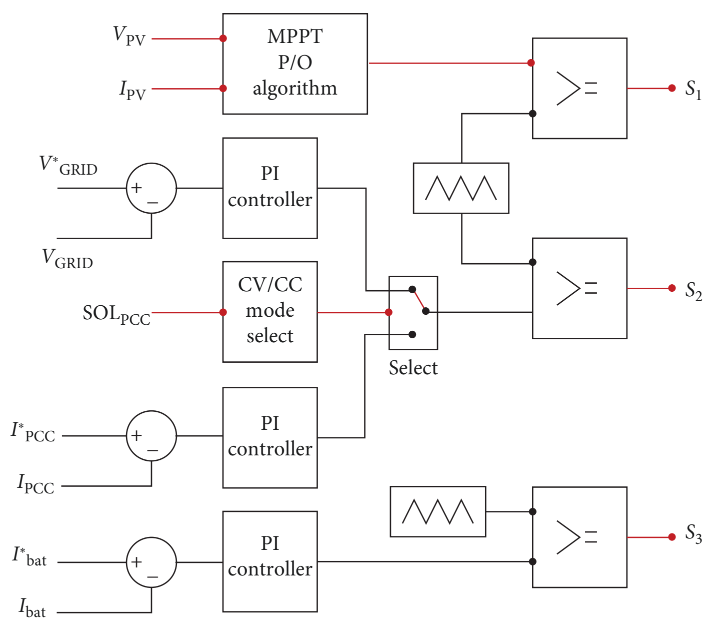


Figure 6: Control loop structure for the proposed system.

to controlled the switch $S_3$. In this strategy, the 180-degree phase angle shift given to the ramp signal for $S_3$, because it creates an alternate charging path.

The CC–CV charging limit for the lithium-ion battery in the proposed system is depicted in Figure 6. It follows a two-stage charging profile, starting with the CC mode and transitioning to the CV mode. In the CC mode, the PI controller limits the average charging level to prevent excessive current flow. Once the battery charge reaches around 90%, the charging mode shifts to CV mode, where the voltage is held constant while the battery continues to charge. The charging limit ensures that the battery is charged efficiently and avoids overcharging.

The proposed converter utilizes a control strategy as depicted in Figure 6. This control strategy serves two main purposes: providing MPPT for the bidirectional MIEC and regulating the output voltage. The control system employs theP&O algorithm as the chosen method for MPPT implementation. To achieve MPPT, the switch $S_1$ is controlled by the duty ratio $d_1$, which is adjusted to yield the maximum power from the photovoltaic sources. The output voltage is regulated by controlling the switch $S_2$ using the duty ratio $d_2$, which enables both charging and discharging of the battery. Additionally, the switch $S_3$ is controlled by the duty ratio $d_3$ to charge the battery from a DC USB power source.

The MPPT P&O algorithm was implemented using a PIC16F88 microcontroller along with a current sensor, specifically the ACS712. Additionally, a potential divider cum voltage sensor was employed for voltage sensing. For the active diode-based voltage multiplier, the construction included the Vishay Si1424EDH-N Channel MOSFET, Vishay Si1499DH P-Channel MOSFET, and the TLV3704 Nano-power comparator. These components were chosen for their specific functionalities and compatibility with the proposed system, enabling the successful implementation of the MPPT algorithm and the voltage multiplier.

## 4. Results and Discussion

*4.1. Simulation Results.* The performance of the bidirectional MIEC was evaluated through a combination of simulation and experimental validation. The authors built the entire system using the MATLAB/SIMULINK environment, allowing them to monitor the converter's performance in simulated scenarios. Simulation results were then analyzed to assess the effectiveness of the MIEC design. Furthermore, the experimental validation involved implementing the converter in real-world conditions to verify its performance and ensure it operates as intended. In the simulations, the assumptions were made that the solar irradiation is constant at 1,000 W/m$^2$, which represents the intensity of the incident solar radiation on the PV source. Additionally, the EMG voltage was assumed to be 1 V, representing the electromyography (EMG) signal voltage used as an input in the energy harvesting system.

The proposed single-stage bidirectional hybrid energy harvesting system operation is being verified by using MATLAB simulations. The simulation concerning the converter executed depending on the control schemes. Let's the assumption made, the solar irradiation is 1,000 W/m$^2$, and EMG voltage is 1 V. Figures 7(a)–7(h) and 8(a)–8(d) displays the different output behaviors of the PV source, EMG, Voltage Multiplier, and USB. Observation made from that the maximum power available in PV ($P_{\mathrm{PV}}$) is 0.605 W (1,000 W/m$^2$), PV Voltage ($V_{\mathrm{PV}}$) is 1.5 V and its current $I_{\mathrm{PV}}$ is 0.4 A. Also observed that the EMG voltage ($V_{\mathrm{EMG}}$) is 1.3 V and voltage taken from the EMG voltage multiplier ($V_{\mathrm{MLT}}$) is 4.2 V.

Case 1 ($0 \leq t < 0.3$ s)

During the initial time period, the USB connected to the DC Source. Therefore the battery charged through the PV, EMG, and also the USB. From the simulation results that the maximum power available in USB ($P_{\mathrm{USB}}$) is 16 W, and its corresponding voltage and the current value are 5 V, 3.2 A, respectively. At the same time, the battery voltage, current, and power observed as 2.51 V, −6.4 A, and 15 W, respectively.

Case 2 ($0.3 \leq t < 0.6$ s)

In this stage, the power getting from PV and EMG stays stable like the previous stage, but the USB disconnected from DC mains. Therefore the USB power ($P_{\mathrm{USB}}$) getting from the simulation result is zero and its open circuit voltage ($V_{\mathrm{USB}}$) is 4.8 V. Also observed that the battery voltage ($V_{\mathrm{bat}}$) is 2.51 V, the battery current ($I_{\mathrm{bat}}$) is 6 A, and its power ($P_{\mathrm{bat}}$) is 0.6 W.

Case 3 ($0.6 \leq t < 0.9$ s)

Let considered, in this period, the PCD connected in USB, and is powered by the sources of PV, EMG, and the battery.

Also, the Figures 7 and 8(a)–8(d) shows the simulated output voltage, output current and output power of the bidirectional multiple input energy harvesting converter. From these results it is found that the maximum power available in USB ($P_{\mathrm{USB}}$) is 13.28 W, and its corresponding voltage and the current value are 4.15 V and 3.2 A, respectively. At this time, the battery voltage, current, and power observed from the simulation 2.47 V, 4 A, and 9.88 W, respectively, which is closely matched the theoretical values.

The simulations resulted in different output behaviors for the PV source, EMG, voltage multiplier, and USB. According to Figures 7 and 8, the maximum power available in the PV source ($P_{\mathrm{PV}}$) was observed to be 0.605 W, considering the solar irradiation of 1,000 W/m$^2$. The PV voltage ($V_{\mathrm{PV}}$) was found to be 1.5 V, and the PV current ($I_{\mathrm{PV}}$) was measured at 0.4 A. Furthermore, the EMG voltage ($V_{\mathrm{EMG}}$) was determined to be 1.3 V, and the voltage obtained from the EMG voltage multiplier ($V_{\mathrm{MLT}}$) was recorded as 4.2 V. These observations provide insights into the behavior and performance of the energy harvesting system under the given conditions.

*4.2. Experimental Implementation of Bidirectional MIEC in Hybrid System.* When selecting components for the proposed system, the main focus was on finding active components with minimal current consumption for the control circuit. This was done to optimize the overall power efficiency of the system. The component choices were based on the system parameters, such as voltage, current, and power requirements. By carefully considering these parameters, components were selected to ensure they meet the specific needs of the system while minimizing power consumption.

The full schematic of the proposed system is shown in Figure 9. This schematic includes the three MOSFETs $S_1$–$S_3$ for bidirectional MIEC and four low-power MOSFET's $S_4$–$S_7$ for vibration energy harvesting. Also, this circuit includes a diode $D_1$, inductor $L_1$ and $L_2$, capacitor $C_1$–$C_4$, comparator, and a control circuit.

The specific component choices of the proposed system discussed here. The main challenge is to find, active components with minimal current consumption for the control circuit. The selection of the components based on the system parameters like voltage current and power.

Figure 9 depicts the experimental setup of the proposed converter. To verify the performance of the proposed converter, choose the PV with open circuit voltage of 1.6 V and short circuit current of 500 mA, the lithium battery voltage of 2.3 V with 6 Ahr, EMG voltage of 1 V, 10 mA, and portable output battery is 3.7 V 1750 mAhr. The MPPT P&O has implemented using PIC16F88 with the current sensor of ACS712 and potential divider cum voltage sensor. The active diode-based voltage multiplier constructed by Vishay Si1424EDH-N Channel MOSFET, Vishay Si1499DH P-Channel MOSFET, and TLV3704 Nano-power comparator. In the proposed control structure, the controller receives the current signal from the battery and uses it to provide the duty ratio $d_3$, which controls the switch $S_3$. The duty

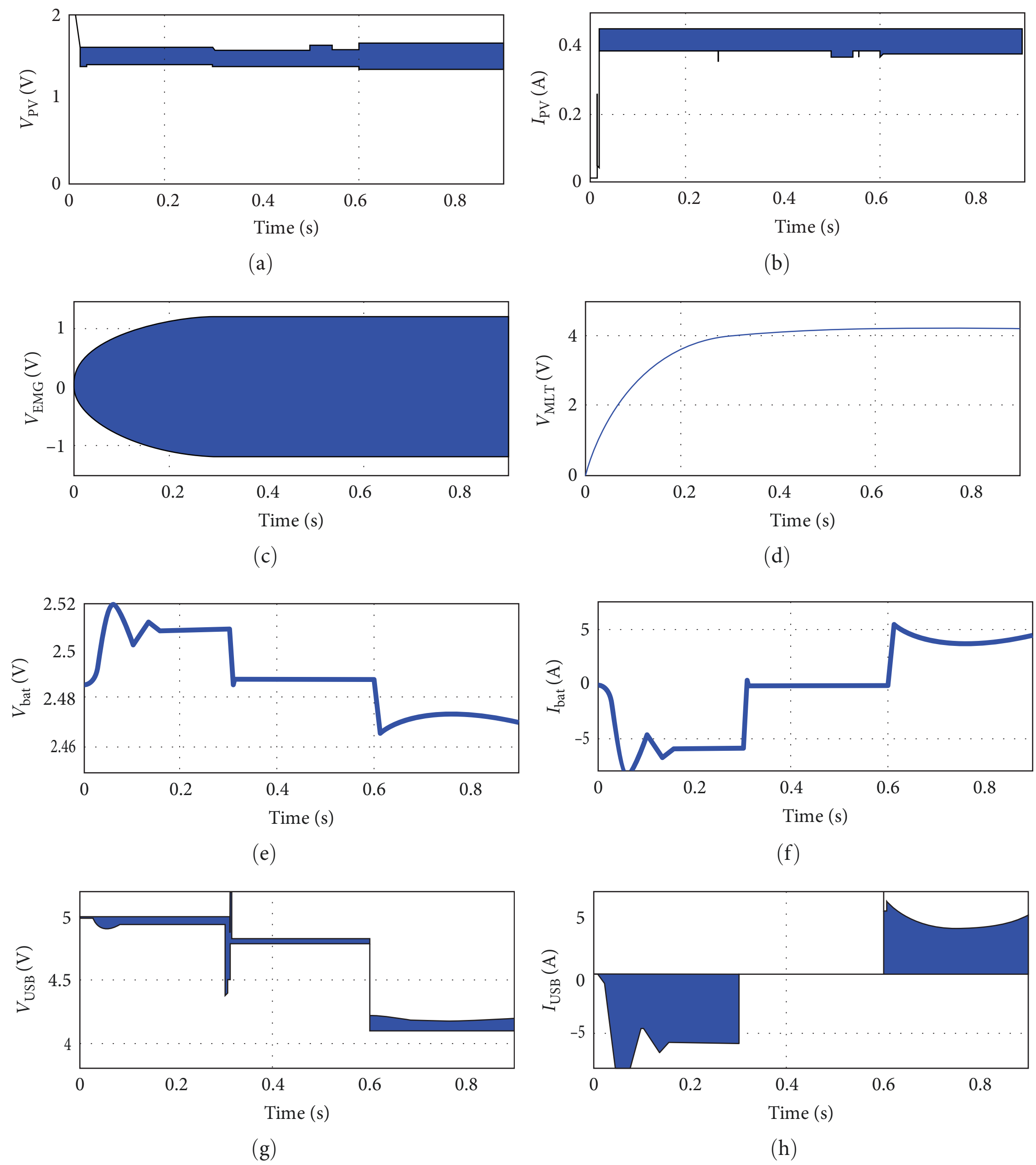


FIGURE 7: Simulation output of voltage and current responses of bidirectional multiple input energy harvesting converter (a–h).

ratio determines the switching pattern of the switch $S_3$, enabling or disabling the charging path for the battery. To create an alternate charging path, the controller introduces a 180-degree phase angle shift to the ramp signal associated with switch S3. This ensures efficient charging control and prevents overcharging of the battery.

The proposed system utilizes a two-stage charge management technique to control the charging of portable devices. When a battery is found to be in an undercharged state, the technique initiates charging in theCC mode. In this mode, a PI controller limits the average charging level of the battery. Once the battery charge reaches around 90%, the charging mode transitions to CV mode. In CV mode, the battery continues to charge, but the controller monitors the charge level to prevent overcharging. When the battery reaches its desired charge level, the controller disconnects it to avoid overcharging.

The experimental setup shown in Figure 9 aimed to verify the performance of the proposed converter. The setup included specific components with the following specifications: a photovoltaic (PV) source with an open circuit voltage of 1.6 V and a short circuit current of 500 mA, a lithium battery with a voltage of 2.3 V, and a capacity of 6 Ahr, an electromyography (EMG) voltage of 1 V and a current of 10 mA, and a portable output battery with a voltage of 3.7 V and a capacity of 1750 mAhr. These components

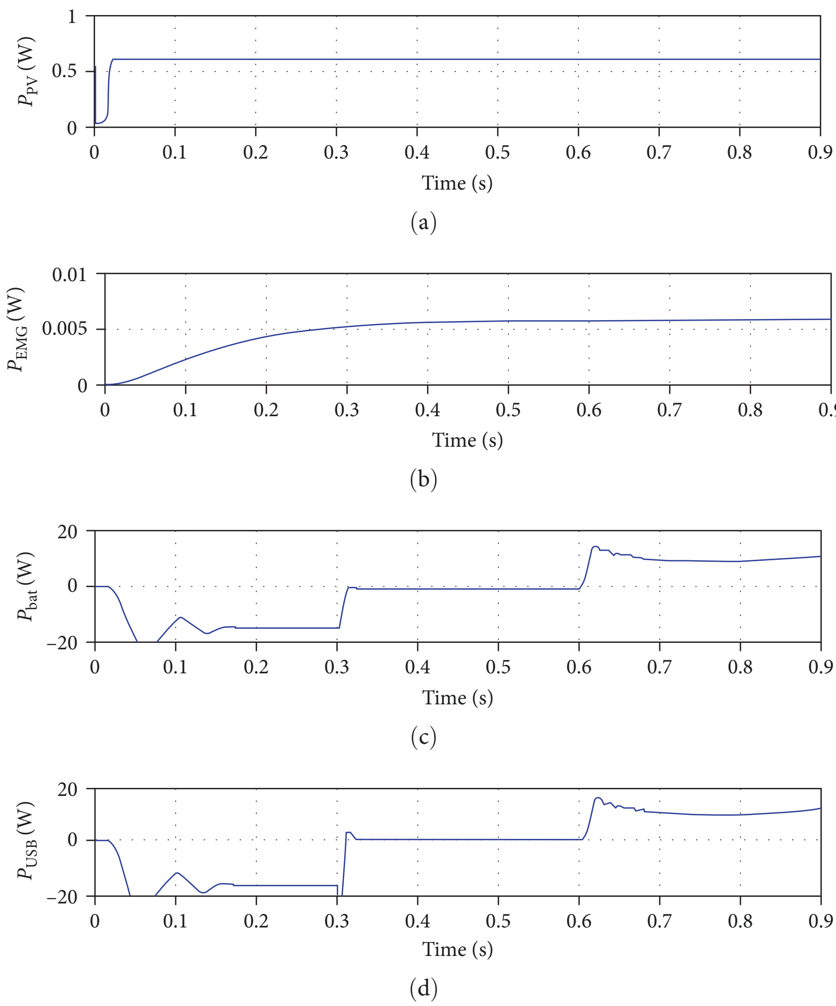


Figure 8: Simulation output of power response of proposed converter (a–d).

were chosen to represent the real-world operating conditions and to evaluate the performance of the converter under these parameters.

*4.3. Power Loss Calculations.* The power losses of the proposed converter are purely depends upon the diode conduction loss, MOSFET conduction loss, and switching loss, other losses which include inductor losses and gate switching loss of the MOSFET.

*4.3.1. Diode Conduction Loss.* The conduction losses in a diode appear when the diode is in forward conduction mode due to the ON-state voltage drop ($V_F$). Most of the time the conduction losses are the main contributor to the total diode power losses and the junction temperature rising ($T_j$).

$$P_{\mathrm{Cond}}\left(T_j\right) = V_{To}\left(T_j\right).\, I_{F(\mathrm{avg})} + R_D\left(T_j\right).\, I^2_{F(\mathrm{RMS})}. \tag{9}$$

$I_{F(\mathrm{avg})}$ is the forward average current

$$I_{F(\mathrm{avg})} = \frac{I_{(\max)} + I_{(\min)}}{2} d, \tag{10}$$

where $I_{\max}$ = maximum forward current; $I_{\min}$ = minimum forward current, $d$ = duty Ratio, and $I_{F(\mathrm{RMS})}$ is the forward root-mean-square (RMS) current flowing through the diode.

$$I_{F(\mathrm{RMS})} = \sqrt{\frac{I^2_{\max} + I^2_{\min} + I_{\max} \times I_{\min}}{3}\, d}. \tag{11}$$

*4.3.2. MOSFET Conduction and Switching Losses.* To calculate conduction losses for MOSFET using Equation (12).

$$\begin{aligned} P_{(\mathrm{Cond})} &= R_{\mathrm{DS(ON)}} \times I^2_{\mathrm{QSW(RMS)}} \\ &= R_{\mathrm{DS(ON)}} \times \frac{V_{\mathrm{OUT}}}{V_{\mathrm{N}}} \times \left(I^2_{\mathrm{OUT}} + \frac{I^2_{\mathrm{ripple}}}{12}\right). \end{aligned} \tag{12}$$

Note that $R$ is the $R_{\mathrm{DS(ON)}}$ of the selected MOSFET. $I$ is the RMS current through the MOSFET, and that neither of these is a function of switching frequency.

MOSFET switching losses are a function of load current and the power supply's switching frequency as shown by

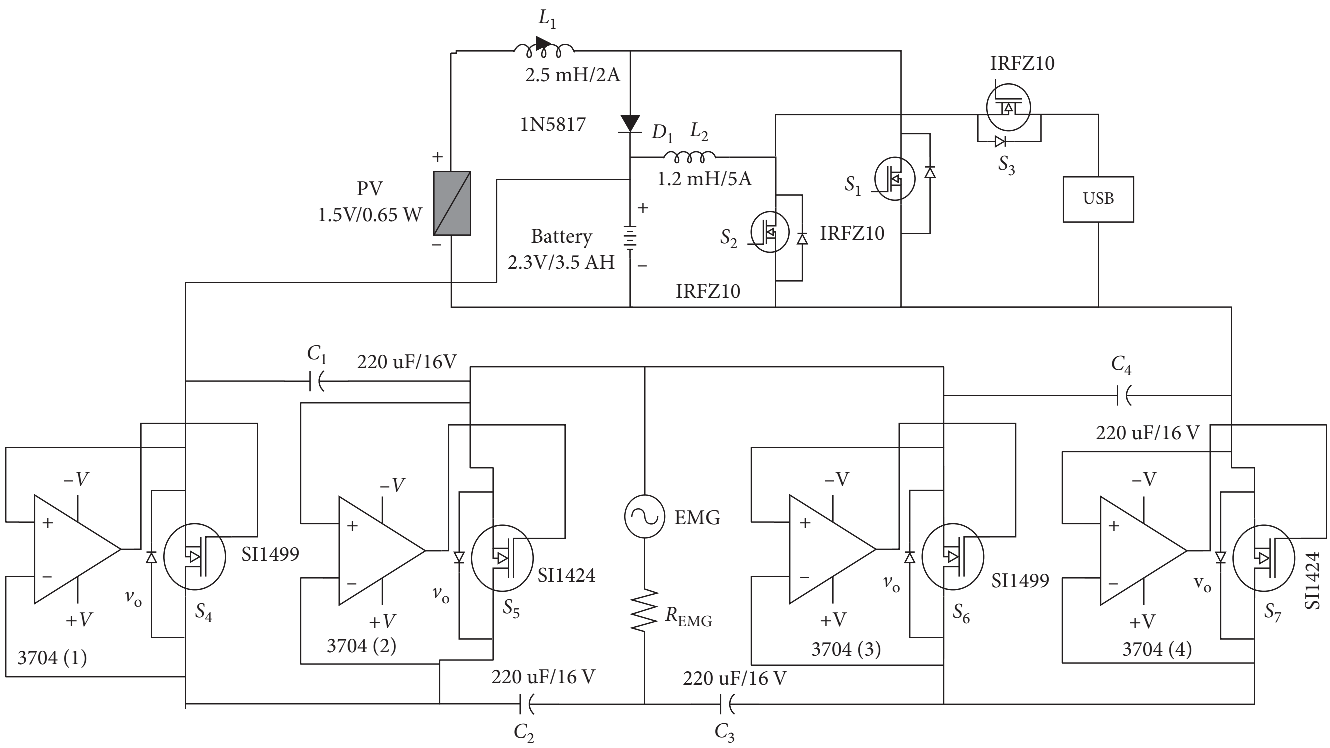


Figure 9: Overall circuit diagram of proposed bidirectional single stage energy harvesting system.

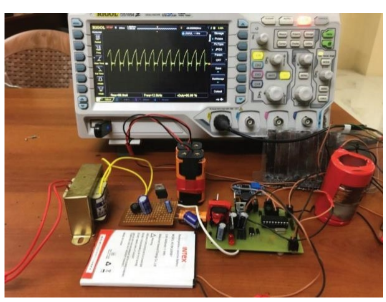

Figure 10: Experimental setup of hybrid system using bidirectional MIEC for portable device charger.

$$P_{SW} = V_{IN} \times I_{OUT} \times f_{SW} \times \frac{(Q_{GS} + Q_{GD})}{I_G}, \quad (13)$$

where $V_{IN} = V_{DS}$ (drain-to-source voltage), $I_{OUT} = I_D$ (drain current), $f_{SW} =$ the switching frequency, $Q_{GS2} =$ gate-to-source charge, $Q_{GD} =$ gate-to-drain charge, and $I_G =$ the gate current.

*4.4. Experimental Analysis of Proposed Hybrid System.* The experimental setup of the proposed converter has been developed as shown in Figure 10. To verify the performance of the proposed converter, PV open circuit voltage of 1.6 V and short circuit current of 500 mA, the lithium-battery voltage is 2.3 V with 6 Ahr, EMG voltage of 1 V, 10 mA, and portable output battery is 3.7 V 1,750 mAhr. The MPPT P&O has implemented using PIC16F88 with the current sensor of ACS712 and potential divider voltage sensor. The voltage multiplier active diode constructed by Vishay Si1424EDH- N Channel MOSFET, VishaySi1499DH P-Channel MOSFET, and TLV3704 Nano-power comparator. The experimental results validated by the different operating conditions. The hardware specifications are given in Table 1.

The first condition tested with the portable device charged by PV power/battery power. Figure 11(a)–11(c) shows the experimental waveform in which the battery discharging current 4.12 A at the voltage of 2.24 V obtained and the output waveform is plotted using the digital storage oscilloscope (DSO). The voltage multiplier-input EMG voltage is 1 V, which produced an output voltage of 3.10 V with low-voltage losses. The sources mentioned above used to charge a portable device battery of charging voltage 3.63 V at an average current 2.51 A.

The test results observed the measured average diode current is 192 mA, RMS diode current is 244 mA. Therefore, the conduction loss in the diode is 79.84 mW also observed that the average body diode current of MOSFET $S_3$ is 2.89 A, and its RMS value is 3.56 A. The MOSFET $S_3$ body diode current is 2.89 A. Therefore, the conduction loss in the body diode of MOSFET $S_3$ is 346.9 mW. Similarly, the voltage and current values of MOSFET $S_1$ and $S_2$ are measured. The RMS value of the voltage and a current of the MOSFET $S_1$ is 1.72 V and 227 mA, with a switching frequency of 9.8 kHz. The RMS value of the voltage and the current of the MOSFET $S_2$ is 3.08 V and 2.92 A with a switching frequency of 9.8 KHz. Hence, the total conduction loss and switching loss of $S_1$ and $S_2$ found as 171.47 mW. The input and output power observed in the system are 9.966 and 9.397 W,

Table 1: Hardware specifications of MIEC converter.

| Specification | Values |
|---|---|
| Photovoltaic panel (6 cells) | |
| Maximum power | 0.65 W |
| Maximum voltage | 1.5 V |
| Maximum current | 435 mA |
| Open circuit voltage | 1.8 V |
| Short circuit current | 483 mA |
| Battery | |
| Battery voltage | 2.3 V |
| Battery capacity | 3500 mAh |
| Full charging voltage | 2.78 V |
| PCD Battery | |
| Battery voltage | 3.8 V |
| Battery capacity | 2600 mAh |
| Full charging voltage | 4.42 V |
| Inductor $L_1$, $L_2$ | 2.5 mH/2 A, 1.2 mH/5 A |
| Diode $D_1$ | IN5817 |
| MOSFET ($S_1 - S_3$) | IRFZ10N |
| P-MOSFET ($S_4 - S_6$) | SI1499DH |
| N-MOSFET ($S_5 - S_7$) | SI1424EDH |
| Comparator | TLV3704 |
| Capacitor($C_1 - C_4$) | EMZR160ARA221MF6 (220 $\mu$F/16 V) |
| Electromagnetic generator | |
| Rated voltage | 1.2 V |
| Rated current | 5 mA |
| Rated power | 6 mW |
| Winding turns | 120 turns/28 gauge |

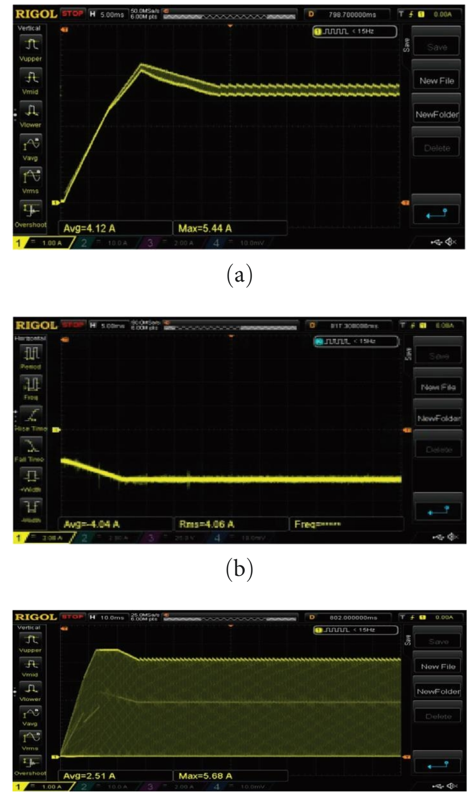


(a)

(b)

(c)

Figure 11: Experimental output waveforms under portable device charging condition: (a) battery current ($I_{\mathrm{bat}}$), (b) portable charging device current ($I_{\mathrm{PCD}}$), and (c) battery average current.

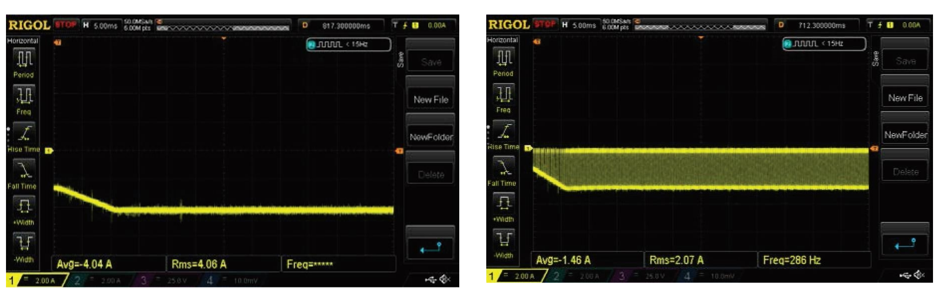


(a) (b)

Figure 12: Experimental output waveform under battery charging condition: (a) battery current ($I_{\mathrm{bat}}$) and (b) USB source current ($I_{\mathrm{USB}}$).

respectively. Therefore, the overall system efficiency of the proposed converter is 94.3%.

The next condition to be tested with, the DC USB to provide the power to charge the battery. Figures 12(a) and 12(b) shows the experimental waveform in which obtained that the battery discharging current of −4.04 A at the voltage of 2.515 V. The voltage multiplier which produced an output voltage of 3.10 V with low-voltage losses. The USB source used to charge the battery with its charging voltage 5 V at an average current 1.46 A.

As like the previous case, the average diode current observed in this condition is 192 mA, and its RMS value is 244 mA. From these values found the conduction loss of diode is 79.84 mW. The average body diode current of MOSFET $S_2$ measured as 1.88 A, and its RMS value is 2.56 A. Therefore, the conduction loss in the body diode of MOSFET $S_3$ is 289 mW. The RMS value of voltage and current of the MOSFET $S_1$ is 1.74 V and 236 mA with a switching frequency of 9.8 kHz. Similarly, the RMS value of the voltage and the current of the MOSFET $S_3$ is 3.32 V and 2.66 A with a switching frequency of 9.8 kHz. Hence, the total conduction loss and switching loss of $S_1$ and $S_3$ found as 243.47 mW. The input and output power observed in the system are −10.785 and −10.35 W, respectively. Therefore,

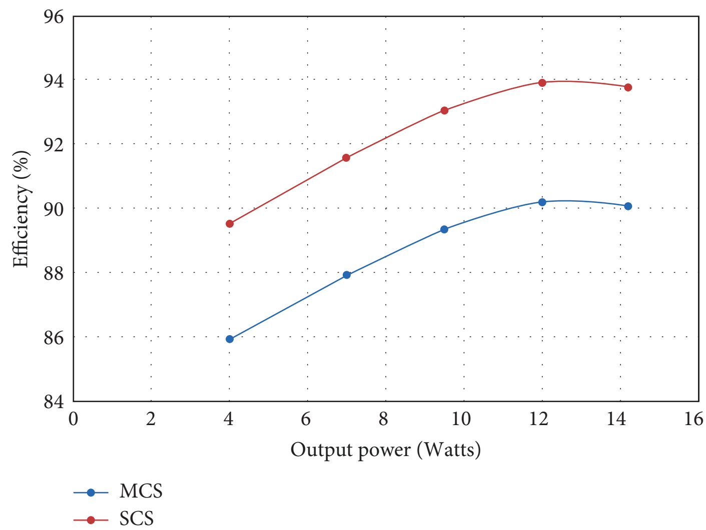


Figure 13: Comparison of measured efficiency vs output power.

Table 2: Comparison of simulation and experimental setup results.

| Parameter | Simulation | Experimental setup |
|---|---|---|
| $P_{PV}$ | 0.605 W | 0.800 W |
| $V_{PV}$ | 1.5 V | 1.6 V |
| $I_{PV}$ | 0.4 A | 0.5 A |
| $V_{EMG}$ | 1.3 V | 1 V |
| $V_{MLT}$ | 4.2 V | 3.1 V |

the overall system efficiency of the proposed converter is 95.96%.

Figure 13 shows the correlation of the output efficiency over the output power of the multistage harvesting system and the proposed single stage harvesting system. As seen, efficiency increases when the output power increases. It is obvious, the single-stage system efficiency is higher than the multistage system because of its reduction in the conversion stage and conduction devices. The simulation and the experimental results comparison of the proposed MIEC converter is illustrated in Table 2.

From Table 2, it is clear that both the simulation and experimental setup results are almost similar and the proposed MIEC converter performs well for the portable device charging applications.

## 5. Conclusions

A single-stage, bidirectional PV/EMG-based MIEC for portable device charging has been conceived, implemented, and tested. The results have also been verified in simulation. The proposed portable charger uses the designed converter to make a hybrid photovoltaic, EMG, and storage systems like the battery. A new power flow path is created by the proposed converter between the low-voltage PV and the PCD. The only way to exchange energy between the battery and PCD in a single power conversion stage is through the bidirectional MIEC. The converter is also equipped with low-power MOSFET and diode components, which facilitates the simple integration with a variety of renewable energy sources. Lower switching losses can be achieved thanks to the converter's numerous voltage-level characteristics. The converter has the advantages of being able to transfer power in both directions and having a relatively basic structure with its low-power components. Verifying the modeling and experimental data demonstrate the effectiveness and dependability of the hybrid system for charging portable electronics.

## Data Availability

The data are used to support the findings of this study are included within the article.

## Disclosure

This study was performed as a part of the Employment of Ramash Kumar K, Department of Electrical and Electronics Engineering, Coimbatore-48, Tamilnadu, India and Rathinamala S, Department of Electrical and Electronics Engineering, KIT-Kalaignarkarunanidhi Institute of Technology, Coimbatore, India.

## Conflicts of Interest

The authors declare that they have no conflicts of interest.

## References

[1] M. Brocanelli and X. Wang, "Making Smartphone smart on-demand for longer battery life," in *IEEE 37th International Conference on Distributed Computing Systems (ICDCS)*, pp. 2288–2293, Atlanta, GA, USA, 2017.

[2] A. D. Joseph, "Energy harvesting projects," *IEEE Pervasive Computing*, vol. 4, pp. 69–71, 2005.

[3] D. Jia, Y. Duan, and J. Liu, "Emerging technologies to power next-generation mobile phone electronic devices using solar energy," *Frontiers of Energy and Power Engineering in China*, vol. 3, pp. 262–288, 2009.

[4] C. Schuss and T. Rahkonen, "Photovoltaic (PV) energy as a recharge source for portable devices such as mobile phones," in *Proceedings of the 12th Conference of FRUCT Association*, pp. 120–128, 2012.

[5] M. Shukman, "Arctic ice melting at 'amazing' speed, scientists find," 2012, http://www.bbc.com/news/world-europe-19508906.

[6] H. S. Thakur and R. N. Patel, "Design and development of dual input DC–DC converter for hybrid energy system," *Journal of Circuits, Systems and Computers*, vol. 28, no. 7, 2019.

[7] L. Solero, A. Lidozzi, and J. A. Pomilio, "Design of multiple-input power converter for hybrid vehicles," in *IEEE Transactions on Power Electronics*, vol. 20, pp. 1007–1016, 2005.

[8] S. Rathinamala and S. Manoharan, "Vibration powered generators and power processing circuits for energy harvesting: a survey," *International Journal of Advanced Research in Electrical, Electronics and Instrumentation Engineering*, vol. 3, no. 5, pp. 9597–9564, 2014.

[9] F. Aymen, "Internal fuzzy hybrid charger system for a hybrid electrical vehicle," *Journal of Energy Resources Technology*, vol. 140, no. 1, 2017.

[10] S. Cheng, R. Sathe, R. D. Natarajan, and D. P. Arnold, "A voltage-multiplying self-powered AC/DC converter with 0.35-V minimum input voltage for energy harvesting applications," *IEEE Transactions on Power Electronics*, vol. 26, no. 9, pp. 2542–2549, 2011.

[11] N. Femia, G. Petrone, G. Spagnuolo, and M. Vitelli, "Optimizing duty-cycle perturbation of P&O MPPT technique," in *IEEE 35th Annual Power Electronics Specialists Conference (IEEE Cat. No.04CH37551)*, vol. 3, pp. 1939–1944, IEEE, Aachen, Germany, 2004.

[12] M. Chen and G. A. Rincon-Mora, "Accurate, compact, and power-efficient li-ion battery charger circuit," in *IEEE Transactions on Circuits and Systems II: Express Briefs*, vol. 53, pp. 1180–1184, IEEE, 2006.

[13] P. C.-P. Chao, W.-D. Chen, and R.-H. Wu, "A battery charge controller realized by a flyback converter with digital primary side regulation for mobile phones," *Microsystem Technologies*, vol. 20, no. 8-9, pp. 1689–1703, 2014.

[14] Y.-S. Kim, G.-C. Park, J.-H. Ahn, and B.-K. Lee, "Hybrid PFC-inverter topology for bidirectional on board charger for range extended electric vehicle," in *18th International Conference on Electrical Machines and Systems (ICEMS)*, pp. 521–524, IEEE, Pattaya, Thailand, 2015.

[15] A. M. Eltamaly and M. A. Mohamed, "8-Optimal sizing and designing of hybrid renewable energy systems in smart grid applications," *Advances in Renewable Energies and Power Technologies*, vol. 2, pp. 231–313, 2018.

[16] T. Porselvi, J. Nisha, K. Thendral, and D. P. Vasantha, "Solar Pv fed electric vehicle charging system with hybrid energy storage system," in *International Conference on Computation of Power, Energy, Information and Communication (ICCPEIC)*, pp. 202–206, IEEE, Melmaruvathur, India, 2019.

[17] C.-M. Lai, Y.-H. Cheng, M.-H. Hsieh, and Y.-C. Lin, "Development of a bidirectional DC/DC converter with dual-battery energy storage for hybrid electric vehicle system," *IEEE Transactions on Vehicular Technology*, vol. 67, no. 2, pp. 1036–1052, 2018.

[18] M. S. Nathan, R. Rajasekaran, and P. U. Rani, "Rules based functional control of bidirectional DC–DC converter for stand-alone PV with hybrid energy storage system," in *International Conference on Innovations in Information, Embedded and Communication Systems (ICIIECS)*, pp. 1–6, IEEE, Coimbatore, India, 2015.

[19] C.-L. Chang and T.-C. Lee, "A compact multi-input thermoelectric energy harvesting system with 58.5% power conversion efficiency and 32.4-mW output power capability," in *2014 International Symposium on Integrated Circuits (ISIC)*, pp. 1–4, IEEE, Singapore, 2014.

[20] A. Agrawal and R. Gupta, "Multi-functional bi-directional DC–DC/AC converter topology for single phase microgrid applications," in *8th IEEE India International Conference on Power Electronics (IICPE)*, pp. 1–6, IEEE, Jaipur, India, 2018.

[21] B. S. N. Raj, R. Siddharth, and S. M. Shyni, "MPPT with bi-directional DC–DC converter and multi-level inverter for grid connected hybrid system," in *International Conference on Computation of Power, Energy Information and Commuincation (ICCPEIC)*, pp. 773–777, IEEE, Melmaruvathur, India, 2017.

[22] H. Khaleghi, A. YazdianVarjani, and M. Mohamadian, "A new bidirectional zeta DC/DC converter," in *The 5th Annual International Power Electronics, Drive Systems and Technologies Conference (PEDSTC 2014)*, pp. 131–136, IEEE, Tehran, Iran, 2014.

[23] M. Sitbon, S. Gadelovits, and A. Kuperman, "Multi-output portable solar charger for Li-ion batteries," in *International Conference on Power Electronics, Machines and Drives (PEMD 2014)*, pp. 1–7, IEEE, Manchester, UK, 2014.

[24] M. Dallard, A. Forest, and A. Shabani, "Design of a portable smart connected solar-powered charger for consumer electronics," in *IEEE 30th Canadian Conference on Electrical and Computer Engineering (CCECE)*, pp. 1–4, IEEE, Windsor, ON, Canada, 2017.

[25] A. Forest, M. Dallard, and A. Shabani, "An optimized platform for performance evaluation of solar battery chargers," in *IEEE 30th Canadian Conference on Electrical and Computer Engineering (CCECE)*, pp. 1–4, IEEE, Windsor, ON, Canada, 2017.

[26] V.-T. Nguyen, T. Pham, T.-H. Luu et al., "High-efficient DC–DC converter based on hybrid SI–SC topology for portable devices," in *International Conference on IC Design and Technology (ICICDT)*, pp. 36–39, IEEE, Hanoi, Vietnam, 2022.

[27] F. M. Shahir, M. Aberoumandazar, and E. Babaei, "Power control of solar cell and stable energy supply by high voltage DC–DC Converter equipped with energy storage," in *2021 International Symposium on Devices, Circuits and Systems (ISDCS)*, pp. 1–5, IEEE, Higashihiroshima, Japan, 2021.

[28] Y. Chen, Y. Zhang, and Y. Liu, "Distributed model predictive control for multi-port DC–DC converter wind-solar complementary system," in *IEEE International Conference on Predictive Control of Electrical Drives and Power Electronics (PRECEDE)*, pp. 789–792, IEEE, Jinan, China, 2021.

[29] S. Sumathi, M. Malukannan, and S. Krishnan, "Analysis of distinctive DC–DC power converters for an enabled freestanding solar water pump," in *2022 International Conference on Power, Energy, Control and Transmission Systems (ICPECTS)*, pp. 1–6, IEEE, Chennai, India, 2022.

[30] J. K. Monny, M. A. Al Noman, R. K. Das, and M. A. Razzak, "Electric vehicle charging station with solar-grid interactive system for maximum power exchange," in *2023 International Conference on Electrical, Computer and Communication Engineering (ECCE)*, pp. 1–6, IEEE, Chittagong, Bangladesh, 2023.

[31] M. Shunmathi, S. J. Fusic, V. Jayshree, K. J. V. Aishwarya, and G. Sharanya, “Solar PV based high gain converter for microgrid applications,” in *2023 Second International Conference on Electronics and Renewable Systems (ICEARS)*, pp. 141–146, IEEE, Tuticorin, India, 2023.

[32] S. Ahmad, A. S. Anees, and J. Bashir, “Design and development of a high gain DC–DC converter suitable for renewable energy application,” in *2023 International Conference on Power, Instrumentation, Energy and Control (PIECON)*, pp. 1–6, IEEE, Aligarh, India, 2023.